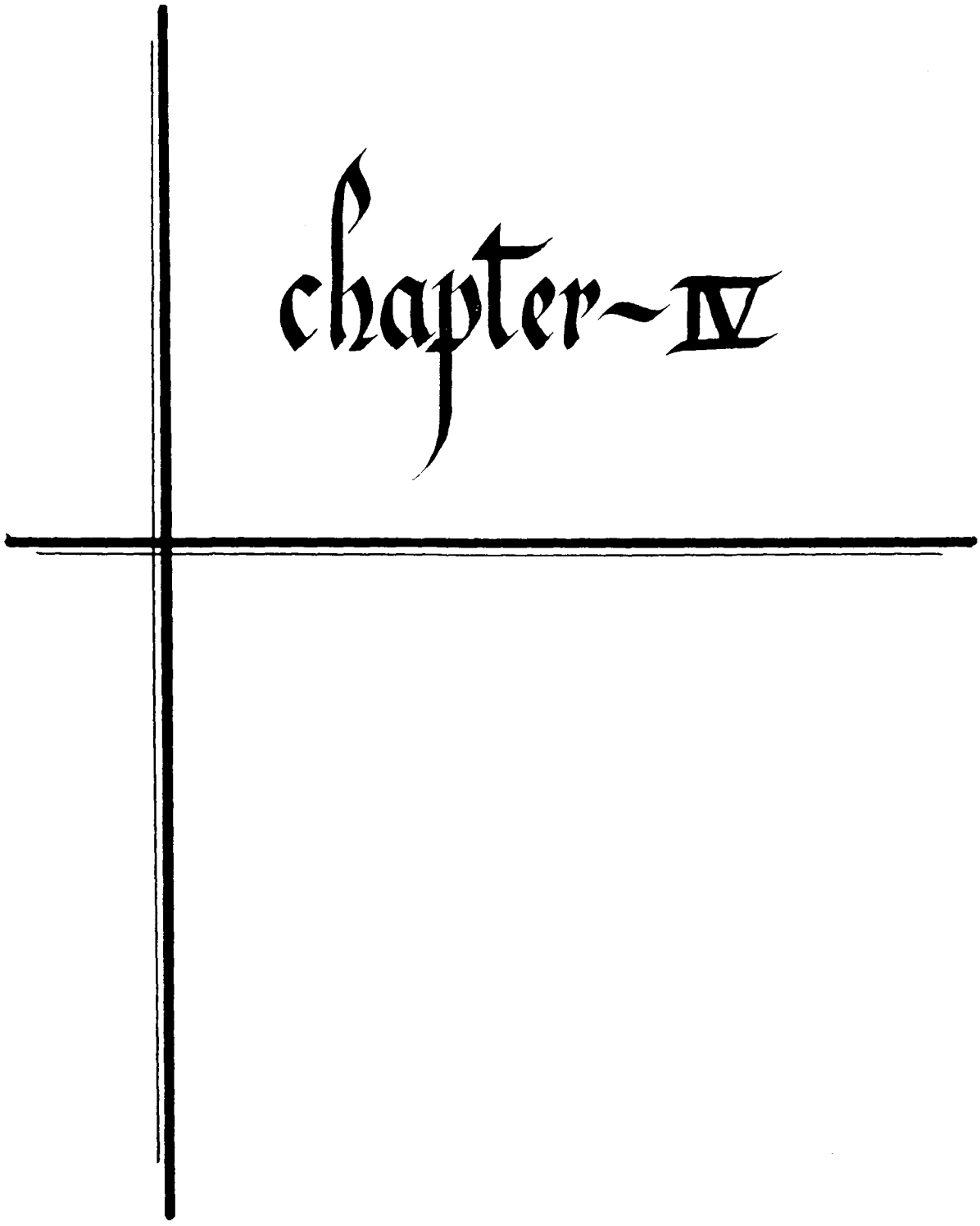
chapter~IV

CHAPTER IV

Thermal and electrical properties of manganese (II) oxalate dihydrate and cadmium (II) oxalate monohydrate

4.1 Introduction

The thermal decomposition of metal oxalate complexes has been studied by numerous workers [1-11] . The decomposition of oxalate complexes is usually complicated and occurs in a series of steps. These steps involve the loss of CO and CO_2, to yield basic carbonate or oxide. The influence of the environment on oxalate decompositions were exothermic in character whereas majority of such decompositions in an inert atmosphere are endothermic [4,12] . The most obvious change caused by the environment is when the actual product is different due to the influence of the surrounding gas atmosphere. The different oxide products was obtained in the case of manganese oxalate decomposition [13-16] . The product in vacuum, nitrogen or any other inert gas is MnO whilst the product in oxygen is one of the other manganese oxides, Mn_2O_3 Mn_3O_4, the exact nature of this product depending on experimental conditions is an example that may be cited [13-18] . The decomposition of cadmium oxalate in air or an inert atmosphere leads to the formation of CdO have also been reported in literature [18,19] . However, the thermal decomposition of

manganese (II) oxalate and cadmium (II) oxalate by using direct current electrical conductivity measurements have not been investigated yet. In continuation of our previous study [20-23] on the thermal decomposition of bivalent transition metal oxalate, this chapter deals with a systematic change of electrical properties and that of ambient atmospheres on thermal decomposition of the manganese (II) oxalate and cadmium (II) oxalates. This study has been supplemented with TGA, DTG and DTA, X-ray diffraction, and infrared spectroscopy.

4.2 Experimental

The procedure for synthesis of manganese (II) oxalate dihydrate ($MnC_2O_4 \cdot 2H_2O$) and cadmium (II) oxalate monohydrate ($CdC_2O_4 \cdot H_2O$) are given in chapter II. The experimental details for the determination of various physical properties viz. infrared spectroscopy, magnetic moment, thermal analyses (TGA, DTG and DTA), X-ray diffraction, and direct current electrical conductivity are explained in Chapter II.

4.3 Results and Discussion

4.3.1 Characterization of $MnC_2O_4 \cdot 2H_2O$ and $CdC_2O_4 \cdot H_2O$

The chemical analyses of $MnC_2O_4 \cdot 2H_2O$ and $CdC_2O_4 \cdot H_2O$ are presented in Table I; it is in good agreement with the

values required by theory. The thermal analysis measurements confirm the presence of water of hydration for these compounds. The infrared spectrum (Fig. 1) of $MnC_2O_4 \cdot 2H_2O$ and $CdC_2O_4 \cdot H_2O$ shows a band at 3420 cm^{-1} due to $\nu_{(OH)}$, an intense band at 1579 cm^{-1} due to $\nu_{asy}(C=O)$ and bands at 1481 cm^{-1} and 1340 cm^{-1} due to $\nu_{sy}(C=O)$. These values indicate the presence of coordinated carboxylate groups [24] . The room temperature magnetic moments (Table I) are very well agrees with the spin only values of Mn^{2+} for $MnC_2O_4 \cdot 2H_2O$, and zero spin of Cd^{2+} for $CdC_2O_4 \cdot H_2O$, which indicates that the compounds have sp^3d^2 hybridization. The polymeric octahedral structure [25,26] have been assigned to these compound. The representative structure is shown in Chapter III, Fig. 2. The insolubility of $MnC_2O_4 \cdot 2H_2O$ and $CdC_2O_4 \cdot H_2O$ in both polar and non-polar solvent is indicative of polymeric structure [26,27] .

4.3.2 Thermal decomposition processes of $MnC_2O_4 \cdot 2H_2O$ and $CdC_2O_4 \cdot H_2O$

(a) Static air atmosphere

$MnC_2O_4 \cdot 2H_2O$

The dehydration step in Fig. 2(a) could be detected in the DTA curve by the presence of endothermic peak at 130 ^oC and a peak was observed at the same temperatures in the DTG curve. The TGA curve showed continuous weight loss around 100-150 ^oC

with a plateau upto 220 °C, corresponding to the loss of two water molecules (Calc. 20.12 %; found, 20.01 %). The temperature variation of the electrical conductivity σ (Fig. 2(b)) did show a initially decrease in conductivity (Region B') upto 95 °C. The X-ray diffraction pattern (Fig. 3(a)) showed broad peaks with no observable change (Table II) [28,29]. This indicates the desorption of physically adsorbed water molecules on the upper surface of the particles. Then there was a constant conductivity between 95 and 226 °C (Region B) corresponds to dehydration process. When the parent compound ($MnC_2O_4 \cdot 2H_2O$) was heated isothermally at 200 °C under this atmosphere, the infrared spectrum revealed no H_2O peak, while the X-ray powder diffraction pattern (Fig. 3(b)) generally showed polycrystallinity with a decrease in interplanar spacings, (Table III) [29] and the elemental analysis agreed with the formula MnC_2O_4 (anhydrous manganese (II) oxalate).

The oxidative decomposition step for $MnC_2O_4 \cdot 2H_2O$ in Fig. 2(a) was observed through the presence of a very strong and broad exothermic peak at 270 °C in the DTA curve. The DTG curve gave a broad peak at 275 °C and the TGA curve showed a continuous weight loss from 230 °C until final recrystallization to Mn_3O_4 (Calc. 46.65 %; found, 46.70 %). After the dehydration process in Fig. 2(b), the σ value started to increase from 226 to 312 °C (Region C), followed by a decrease and then

sharp increase σ upto 350 °C (Region D). Later, σ remained almost constant in the temperature range 350-400 °C (Region E). When $MnC_2O_4 \cdot 2H_2O$ was heated isothermally at 290 °C, the infrared spectrum demonstrated decreases in the intensities of the coordinated oxalate bands, and bands occurred at 604 cm^{-1} (m) and 475 cm^{-1} (m) for the metal-oxygen stretching frequencies due to the presence of the manganese oxide formed [30] . The X-ray diffraction pattern indicated (Fig. 3(c)) that this sample was polycrystalline in nature; peaks corresponding to both MnO [31] and MnC_2O_4 were observed (Table IV). Even though a tendency to a sharp increase in σ was observed at 331 °C (Region D), the characteristics value of Mn_3O_4 ($\sim 10^{-6} ohm^{-1} cm^{-1}$) could be obtained under dynamic condutions. However, the X-ray diffraction (Fig. 3(d)) studies confirmed mainly to Mn_3O_4 and traces of MnO were formed at this temperature. The infrared spectrum of the parent sample heated at 340 °C showed no bands due to coordinated carboxylate, but strong bands of Mn-O stretching frequencies were observed. Above 400 °C (Region E), X-ray diffraction pattern (Fig. 3(c)) showed mainly Mn_3O_4 (Table V) [32] ; the sample is brownish black and crystalline. The sample thus obtained at 400 °C shows a change in σ as the temperature is changed (see cooling and heating cycle, Fig.2(b)). This behaviour is characteristic of Mn_3O_4 and it has tetragonally deformed spinel [33] .

$\underline{CdC_2O_4 \cdot H_2O}$

Thermal analysis (TGA, DTG and DTA) of cadmium (II) oxalate ($CdC_2O_4 \cdot H_2O$) are given in Fig. 2(c). It can be seen from TGA curve that a weight loss beginning at 90-195 ^{o}C with a plateau upto 340 ^{o}C, corresponded to the removal of the water molecule contained in this oxalate (Calc. 8.24 %; found, 8.35%). The DTA curve produced a broad endothermic peak and DTG peak also observed at the same temperature, corresponding to the loss of one water molecule, in this temperature range. This dehydration step was also clearly indicated by a steady decrease in σ in Region B' and then remained nearly constant in Region B (upto 330 ^{o}C) of the log σ vs. T^{-1} plot (Fig. 2(d)). The $CdC_2O_4 \cdot H_2O$ sample heated isothermally under static air at 260 ^{o}C, showed no H-OH bands in infrared spectrum and the X-ray diffraction pattern (Fig. 4(b)) showed broad peaks with a decrease in interplanar spacing (Table III). The elemental analysis also agreed well with the anhydrous oxalate (CdC_2O_4) formation. Thus, Region B' and B was therefore said to correspond to the dehydration of $CdC_2O_4 \cdot H_2O$.

An exothermic peak at 395 ^{o}C was seen in the DTA curve and also a broad peak at the same temperature on the DTG curve corresponding to the oxidative decomposition of CdC_2O_4 (Fig. 2(c)). The TGA curve showed a continuous weight loss

from 340 °C until the sample crystallization to CdO occurred (Calc., 35.93 %; found 36.71 %). The plot of log σ vs. T^{-1} clearly showed the different intermediate phases which occurred during the decomposition. The value of σ steadily increased from 352 to 440 °C (Region C) and the infrared spectrum of the isothermally heated $CdC_2O_4 \cdot H_2O$ sample at 390 °C showed a decrease in intensity of coordinated carboxylate bands, in addition, bands at 605 cm^{-1} (m), 487 cm^{-1} (s) and 462 cm^{-1} (m) occurred for metal-oxygen stretching frequencies due to presence of cadmium oxide [30]. The X-ray diffraction pattern (Fig. 4(c)) of this isothermally heated sample (Table VI) showed the structure to be polycrystalline in nature; the peaks corresponding to both CdC_2O_4 and CdO [34] were observed. The infrared spectrum and X-ray diffraction pattern in Fig. 4(d) for the sample decomposed isothermally at 500 °C (Region D) showed mainly CdO (Table VII), the sample was brown and had an electrical conductivity value of about 10^{-5} $\Omega^{-1}cm^{-1}$ [35]. The sample thus obtained at 510 °C showed intrinsic semiconducting properties i.e. a variation in σ with variation of temperature. This behaviour is characteristic CdO [35].

It is well known that [17,18] the temperature and the mechanism of the oxalate was altered by the surrounding atmosphere. Hence, it is important to compare the data obtained

under the atmosphere with the data obtained under different atmospheres.

(b) Dynamic dry nitrogen atmosphere

$MnC_2O_4 \cdot 2H_2O$

The TGA curve in (Fig. 5(a)) showed the loss of two water molecules at 120-165 °C with a plateau upto 320 °C; the DTA curve exhibited a single endothermic peak at 130 °C, and the DTG curve one at 135 °C. These thermal curves therefore indicated single-step dehydration under this atmosphere. However, Region B of the plot of log σ vs. T^{-1} showed in Fig. 5(b) can be related to dehydration of $MnC_2O_4 \cdot 2H_2O$. Hence, it can be said that the direct current electrical conductivity measurements provide a more detailed picture of the thermal process. Isothermal heating of the parent compound at 225 °C showed its polycrystalline nature as revealed by its X-ray diffraction pattern (similar to Fig. 3(b)), and the elemental analysis fitted well to the formula MnC_2O_4 [29].

An endothermic peak was observed at 410 °C in DTA curve and in the DTG at the same temperature corresponding to thermal decomposition. The TGA curve (Fig. 5(a)) showed a continuous weight loss from 320 to 430 °C. Thus weight loss was found to be good agreement with the formation of MnO as a

final product (Calc., 50.36 %; found, 50.21 %). The plot of log σ vs. T^{-1} (Fig. 5(b)) showed a decrease and then steep increase in σ at 316-405 °C (Region C) and then remained constant above this temperature (Region D). The infrared spectrum of the isothermally heated parent compound in Region C showed increase in intensity of Mn-O stretching frequencies and a decrease in frequency for the coordinated carboxylate bands. The X-ray diffraction pattern revealed MnO [31] was present in this stage together with some MnC_2O_4 (Fig. 3(c)). The infrared spectrum and X-ray diffraction pattern (Fig. 3(f)) for the sample decomposed isothermally at 450 °C showed mainly MnO (Table VII) [31] ; the sample was grayish green. No line which could be assigned to metallic manganese was detected in our work. The sample thus obtained at 450 °C shows a variation in σ with temperature. This behaviour is a characteristic of the non-stoichiometry present in MnO [33] .

$\underline{CdC_2O_4 \cdot H_2O}$

The TGA curve of cadmium (II) oxalate monohydrate ($CdC_2O_4 \cdot H_2O$) showed the first stage due to dehydration at ~150 °C (Fig. 5(c)). This step was also indicated by an endothermic peak in DTA at 125 °C and a broad peak at same temperature on DTG curve. Region B' and B in the plots of

log σ vs. T^{-1} (Fig. 5(d)), correspond to the dehydration of $CdC_2O_4 \cdot H_2O$. The isothermally heated sample of $CdC_2O_4 \cdot H_2O$ at 240 °C under dynamic nitrogen atmosphere was found to be less crystalline as shown from the X-ray diffraction pattern (Table III), while the infrared spectrum showed no H-OH band. The elemental analysis agreed well with the anhydrous compound complete (CdC_2O_4).

The decomposition steps of the CdC_2O_4 was indicated by an endothermic peak in the DTA curve at 415 °C and in the DTG curve at same temperature. The TGA curve showed a rapid stage of decomposition (Fig. 5(c)). The decomposition was completed by ~ 450 °C. The composition of the final product at this temperature was CdO. The plot of log σ vs. T^{-1} (Fig. 5(d)) showed a steady increase in values of σ in the temperature range 250-380 °C (Region C). The infrared spectrum and X-ray diffraction pattern (similar to Fig.4(c)) for sample heated isothermally at 360 °C showed that CdO [34] was present in this stage together with some CdC_2O_4. A steep increase in σ has been observed in Region D corresponding to CdO formed as the final product. X-ray diffraction analysis (Fig. 4(d)) has confirmed the formation of this phase (Table VII). No line which can be assigned to metallic cadmium could be detected.

Although the decomposition behaviour was mostly the same in static air and dynamic dry nitrogen atmospheres some critical differences were observed. These differences could be clarified when the study was carried out under dynamic air atmosphere.

(c) Dynamic air atmosphere

$MnC_2O_4 \cdot 2H_2O$

The dehydration step observed in Fig. 6 (a) gave a single endothermic peak at 125 ^{o}C in DTA curve; at this temperature the DTG curve also showed a peak. The TGA curve displayed a continuous weight loss upto 170 ^{o}C, with a plateau at 230 ^{o}C (Fig. 6(a)). The weight loss upto 170 ^{o}C corresponds to the loss of two water molecules. However, in Fig. 6(b) the plot of log σ vs. T^{-1} showed Region B' and B, indicating dehydration steps quite clearly.

The DTA curve contained broad exothermic peaks at 290 ^{o}C correspond to oxidative decomposition. The DTG curve included a broad peak at 280 ^{o}C, and TGA curve showed continuous weight loss from 230 to 330 ^{o}C, where the material finally crystallized to Mn_3O_4. Supplementing direct current electrical conductivity measurements (Fig. 6(b)) revealed definite regions of conductivity corresponding to the various

intermediates formed. The isothermal decomposition study under the atmosphere demonstrated that the intermediates were similar to those obtained under the static air atmosphere (see Fig. 2(b)).

$\underline{CdC_2O_4 \cdot H_2O}$

The TGA curve showed a continuous weight loss between 85 and 230 °C (Fig. 6(c)). The DTG curve showed a broad peak at 140 °C. The DTA curve showed an endothermic peak at 135 °C corresponding to the dehydration of $CdC_2O_4 \cdot H_2O$ and an exothermic peak at 380 °C corresponding to oxidative decomposition. The TGA showed a continuous weight loss from 350 °C until it crystallized to CdO.

Region B in the plot of log σ vs. T^{-1} (Fig. 6(d)) corresponds to the dehydration of $CdC_2O_4 \cdot H_2O$. There was a steady increase in the value of σ between 340 and 410 °C (Region C), then there was a steep increase in values of σ in the temperature range 410-510 °C (Region D). The infrared and the X-ray diffraction for the sample decomposed isothermally at 380 °C and 500 °C showed CdO along with anhydrous CdC_2O_4 and pure CdO [34] respectively.

Polar gases were obtained at around 350 °C on the thermal decomposition of the parent compound under a dynamic

nitrogen atmosphere, and are observed by qualitative gas detection method. The detail detection procedure is described in Chapter III.

The predicted intermediates obtained in each temperature region under all the above atmosphere are shown in Table VIII and IX. The final product obtained by the decomposition of $MnC_2O_4 \cdot 2H_2O$ was always Mn_3O_4 in static and dynamic air atmosphere. These reactions are present as follows :

$$MnC_2O_4 \cdot 2H_2O \xrightarrow{40\text{-}226\,^{\circ}C} MnC_2O_4 + 2H_2O\uparrow \quad .. \quad (1)$$

$$MnC_2O_4 \xrightarrow{226\text{-}312\,^{\circ}C} MnO + CO\uparrow + CO_2\uparrow \quad .. \quad (2)$$

$$2MnO + MnC_2O_4 \xrightarrow{312\text{-}400\,^{\circ}C} Mn_3O_4 + 2CO\uparrow \quad .. \quad (3)$$

The transformation of MnC_2O_4 to MnO was the final step detected in a dynamic dry nitrogen atmosphere, while CdC_2O_4 transformed to CdO under static air, dynamic dry nitrogen and dynamic air atmospheres :

$$CdC_2O_4 \cdot H_2O \xrightarrow{40\text{-}330\,^{\circ}C} CdC_2O_4 + H_2O\uparrow \quad .. \quad (4)$$

$$2CdC_2O_4 \xrightarrow{330\text{-}410\,^{\circ}C} CdC_2O_4 + CdO + CO\uparrow + CO_2\uparrow \quad .. \quad (5)$$

$$CdC_2O_4 + CdO \xrightarrow{410\text{-}520\,^{\circ}C} 2CdO + CO\uparrow + CO_2\uparrow \quad .. \quad (6)$$

4.4 Conclusions

The present study revealed the following findings on the solid-state dehydration and decomposition of $MnC_2O_4 \cdot 2H_2O$ and $CdC_2O_4 \cdot H_2O$.

(a) The oxidative decomposition behaviour of $MnC_2O_4 \cdot 2H_2O$ and $CdC_2O_4 \cdot H_2O$ were better understood from the study of the direct current electrical conductivity measurements, which showed different regions of conductivity for the intermediates formed, whereas the oxidative decomposition behaviour could not be clearly understood from the thermal curves.

(b) The final product of decomposition in static air and dynamic air was found to be Mn_3O_4 for $MnC_2O_4 \cdot 2H_2O$. However, the final decomposition product in all three atmospheres was found to be CdO for $CdC_2O_4 \cdot H_2O$.

(c) Qualitative gas analyses showed that carbon monoxide and carbon dioxide gases were present during the thermal decomposition of $MnC_2O_4 \cdot 2H_2O$ or $CdC_2O_4 \cdot H_2O$.

4.5 References

1. J.E. House Jr., Thermochim. Acta, 47 (1981) 71.
2. J.E. House Jr., Thermochim. Acta, 43 (1981) 237.
3. D. Dollimore and D.L. Griffiths, J. Chem. Anal., 2 (1970) 229.
4. D.A. Young, Decomposition of Solids, (Pergamon Press, Oxford, 1966) P. 77, 148 and 152.
5. W.W. Wendlandt and E.L. Simon, J. Inorg. Nucl. Chem., 27 (1965) 2317 and 2325.
6. W.W. Wendlandt and E.L. Simon, Thermochim. Acta, 2 (1971) 217.
7. N. Tanaka and K. Sato, Bull. Chem. Soc. Jpn., 43 (1970) 789.
8. K. Nagase, Bull. Chem. Soc. Jpn, 45 (1972) 2166.
9. N. Tanaka and M. Nanjo, Bull. Chem. Soc. Jpn, 40 (1967) 330.
10. W.W. Wendlandt and E.L. Simons, J. Inorg. Nucl. Chem., 28 (1968) 2420.
11. J.D. Danforth and J. Dix, Inorg. Chem., 10 (1971) 1623.
12. W.E. Garner, Chemistry of the Solid State (Butterworths, 1955) P.232.
13. D. Dollimore, J. Dollimore and J. Little, J. Chem. Soc., (1969) 2946.
14. M. Brown, D. Dollimore and A.K. Galwey, J. Chem. Soc. Faraday Trans. I, 70 (1974) 1316.

15. D. Dollimore, J. Therm. Anal., 11 (1977) 185.

16. D. Dollimore, Thermochim. Acta, 117 (1987) 331-363.

17. E.D. Macklen, J. Inorg. Nucl. Chem., 30 (1968) 2689.

18. D. Dollimore, D.L. Griffiths and D.Nicholson, J. Chem. Soc.,(1963) 2617.

19. C. Duval, "Inorganic Thermogravimetric Analysis", (Elsevier, Amsterdam, 1953) P. 531.

20. K.S. Rane, A.K. Nikumbh and A.J. Mukhedkar, J. Mater. Sci., 16 (1981) 2387.

21. A.K. Nikumbh, M.M. Phadke, S.K. Date and P.P. Bakare, Thermochim. Acta, 239 (1994) 253.

22. A.K. Nikumbh, M.M. Rahman and A.D. Aware, Thermochim. Acta, 159 (1990) 109.

23. A.K. Nikumbh, A.E. Athare and V.B. Raut, Thermochim. Acta, 186 (1991) 217.

24. K. Nakamoto, Infrared Spectra of Inorganic and Coordinated Compounds, (Wiley-Interscience, New York, 2nd edn., 1970).

25. C.P. Prabhakaran and C.C.Patel, Indian J. Chem., 7 (1969) 266.

26. J.R. Allan, N.D. Baird and A.L. Kassyk, J. Therm. Anal., 16 (1979) 79.

27. J.R. Allan, J.G. Bonner, H.J. Bowley, D.L. Gerrard and S. Hoey, Thermochim. Acta, 141 (1989) 227.

28. ASTM File Number 25-544.

29. J. Robin, Bull. Soc. Chim. Fr. (1953) 1078.

30. N.T. Mcdevitt and L. B. William, Spectro. Chemica. Acta, 20 (1964) 799.

31. ASTM File Number 7-230.

32. ASTM File Number 24-734

33. D.J. Craik, Magnetic Oxides, Vol. 1 (Wiley Interscience, New York, 1975) P.450 and 466.

34. ASTM File Number 5-640.

35. J.C. Bailar, H.J. Emeleus, Sir R. Nyholm and A.F. Trotman-Dickenson, 'Comprehensive Inorganic Chemistry', Vol. 3, (Pergamon Press, 1973) P. 266.

Table I : Analytical data of manganese (II) oxalate dihydrate ($MnC_2O_4 \cdot 2H_2O$) and cadmium (II) oxalate monohydrate ($CdC_2O_4 \cdot H_2O$)

Compound	Formula	Formula weight	Elemental analysis in wt.%						Magnetic moment (μ) B.M.
			C		H		Metal		
			Calc.	Found	Calc.	Found	Calc.	Found	
Manganese (II) oxalate dihydrate (Colour - White)	$MnC_2O_4 \cdot 2H_2O$	178.92	13.41	13.48	2.24	2.29	30.71	29.80	5.71
Cadmium (II) oxalate monohydrate (Colour - White)	$CdC_2O_4 \cdot H_2O$	218.41	10.99	11.66	0.92	0.98	51.47	50.10	Zero

Table II : X-ray diffraction data of $MnC_2O_4 \cdot 2H_2O$ and $CdC_2O_4 \cdot H_2O$[a]

Observed d-spacing[b] for $MnC_2O_4 \cdot 2H_2O$ (^oA)	Observed d-spacing for $CdC_2O_4 \cdot H_2O$ (^oA)
4.79 (100)	4.66 (8)
4.67 (60)	4.22 (7)
3.86 (28)	3.86 (100)
3.63 (49)	3.49 (14)
2.98 (87)	2.97 (13)
2.84 (25)	2.79 (18)
2.63 (60)	2.59 (18)
2.39 (15)	2.39 (40)
2.28 (53)	2.31 (51)
2.12 (27)	2.13 (38)
2.03 (28)	1.93 (38)
1.99 (28)	1.76 (64)
1.92 (53)	1.68 (30)
1.84 (84)	1.60 (31)
1.74 (32)	1.56 (27)
1.71 (23)	1.49 (36)
1.68 (20)	1.45 (33)
1.61 (19)	1.28 (27)
1.55 (24)	1.23 (31)
1.50 (21)	1.20 (46)
1.46 (32)	1.12 (38)
1.42 (25)	

a. The figures in parentheses are intensities relative to the linewidth intensity (100).

b. Ref. 28.

Table III : X-ray diffraction data for anhydrous MnC_2O_4 and CdC_2O_4 obtained from $MnC_2O_4 \cdot 2H_2O$ and $CdC_2O_4 \cdot H_2O$ by heating in an atmosphere of nitrogen at 225 °C and 260 °C respectively[a]

Observed d-spacing[b] for MnC_2O_4 (°A)	Observed d-spacing for CdC_2O_4 (°A)
6.31 (100)	6.32 (48)
5.85 (43)	6.10 (12)
5.51 (35)	5.21 (18)
3.73 (48)	3.86 (100)
3.57 (29)	3.18 (10)
2.83 (39)	2.92 (18)
2.86 (32)	2.71 (16)
2.76 (20)	
2.25 (24)	2.56 (36)
2.07 (32)	2.49 (8)
1.95 (30)	2.37 (18)
1.82 (27)	2.27 (14)
1.77 (27)	2.05 (10)
1.47 (24)	1.95 (14)
1.42 (24)	1.80 (14)
	1.68 (10)
	1.47 (6)

a. The figures in parentheses are intensities relative to the linewidth intensity (100).

b. Ref. 29.

Table IV : X-ray diffraction data for MnC_2O_4 and MnO obtained from $MnC_2O_4 \cdot 2H_2O$ by heating in an atmosphere of static air at 290 ^oC[a]

Observed d-spacing (^oA)	MnO d-spacing[b] (^oA)
6.28 (60)	
5.91 (28)	
5.21 (17)	
3.73 (25)	
3.04 (10)	
2.63 (40)	2.568 (60)
2.39 (12)	
2.15 (100)	2.223 (100)
2.07 (15)	
1.95 (15)	
1.78 (10)	
1.54 (40)	1.571 (60)
1.47 (21)	
1.35 (10)	1.340 (20)
1.28 (10)	1.283 (14)
	1.112 (12)
	1.019 (10)
	0.994 (18)
	0.907 (16)
	0.855 (14)
	0.786 (4)

a. The figures given in parentheses are intensities relative to the linewidth intensity (100).

b. Ref. 31.

Table V : X-ray diffraction data for Mn_3O_4 obtained from $MnC_2O_4 \cdot 2H_2O$ by heating in an atmosphere of static air at 360 °C[a]

Observed d-spacing (°A)	Mn_3O_4 d-spacing[b] (°A)
4.98 (40)	4.924 (30)
3.12 (41)	3.089 (40)
2.88 (26)	2.881 (17)
2.79 (76)	2.768 (85)
2.50 (100)	2.487 (100)
2.43 (25)	2.463 (20)
2.36 (32)	2.367 (20)
2.04 (25)	2.037 (20)
	1.828 (07)
1.80 (31)	1.798 (25)
1.69 (15)	1.700 (10)
	1.64 (8)
1.56 (28)	1.57 (25)
1.50 (55)	1.52 (50)
	1.47 (3)
1.42 (40)	1.44 (20)
	1.277 (10)

a. The figures given in parentheses are intensities relative to the linewidth intensity (100).

b. Ref. 32.

Table VI : X-ray diffraction data for CdC_2O_4 and CdO obtained from $CdC_2O_4 \cdot H_2O$ by heating in an atmosphere of static air at 390 °C[a]

Observed d-spacing (°A)	CdO d-spacing[b] (°A)
6.33 (33)	
5.25 (9)	
3.89 (73)	
2.95 (10)	
2.74 (100)	2.712 (100)
2.60 (24)	
2.35 (61)	2.349 (88)
2.29 (7)	
1.92 (8)	
1.67 (38)	1.661 (43)
1.42 (20)	1.416 (28)
1.30 (18)	1.335 (13)
1.05 (16)	1.049 (9)
0.96 (16)	0.958 (11)
0.91 (15)	0.903 (9)
	0.830 (5)

a. The figures given in parentheses are intensities relative to the linewidth intensity (100).

b. Ref. 34.

Table VII : X-ray diffraction data for MnO and CdO obtained from $MnC_2O_4 \cdot 2H_2O$ and $CdC_2O_4 \cdot H_2O$ by heating in an atmosphere of nitrogen at 450 °C and 500 °C respectively[a]

Observed d-spacing for MnO (°A)	Observed d-spacing for CdO (°A)
2.60 (50)	2.76 (100)
2.18 (100)	2.33 (76)
1.60 (45)	1.69 (40)
1.36 (28)	1.43 (33)
1.26 (20)	1.33 (21)
1.10 (15)	1.06 (11)
1.02 (11)	0.96 (18)
0.99 (27)	0.90 (13)
0.91 (23)	
0.86 (18)	

a. The figures given in parentheses are intensities relative to the linewidth intensity (100).

Table VIII : Predicted intermediates and final product obtained from $MnC_2O_4 \cdot 2H_2O$ under different atmospheres, measured via direct current electrical conductivity

Atmosphere	Region	Temperature ranges, ^oC	Predicted intermediates and final products
Static air	A	30 - 60	$MnC_2O_4 \cdot 2H_2O$
	B'	60 - 95	$MnC_2O_4 \cdot H_2O$
	B	95 - 226	MnC_2O_4
	C	226 - 312	$MnO + MnC_2O_4$
	D	331 - 250	$MnO + Mn_3O_4$
	E	350 - 400	Mn_3O_4
Dynamic nitrogen	B'	50 - 83	$MnC_2O_4 \cdot H_2O$
	B	83 - 282	MnC_2O_4
	C	316 - 405	$MnO + MnC_2O_4$
	D	405 - 450	MnO
Dynamic air	B'	65 - 83	$MnC_2O_4 \cdot H_2O$
	B	83 - 225	MnC_2O_4
	C	225 - 316	$MnO + MnC_2O_4$
	D	330 - 360	$MnO + Mn_3O_4$
	E	above 360	Mn_3O_4

Table IX : Predicted intermediates and final product obtained from $CdC_2O_4 \cdot H_2O$ under different atmospheres, measured via direct current electrical conductivity.

Atmosphere	Region	Temperature ranges, °C	Predicted intermediates and final products
Static air	A	30 - 70	$CdC_2O_4 \cdot H_2O$
	B'	70 - 180	CdC_2O_4
	B	180 - 330	
	C	352 - 440	$CdO + CdC_2O_4$
	D	440 - 520	CdO
Dynamic nitrogen	B'	65 - 165	CdC_2O_4
	B	165 - 250	
	C	250 - 380	$CdO + CdC_2O_4$
	D	380 - 470	CdO
Dynamic air	B'	60 - 170	CdC_2O_4
	B	170 - 280	
	C	280 - 400	$CdO + CdC_2O_4$
	D	400 - 480	CdO

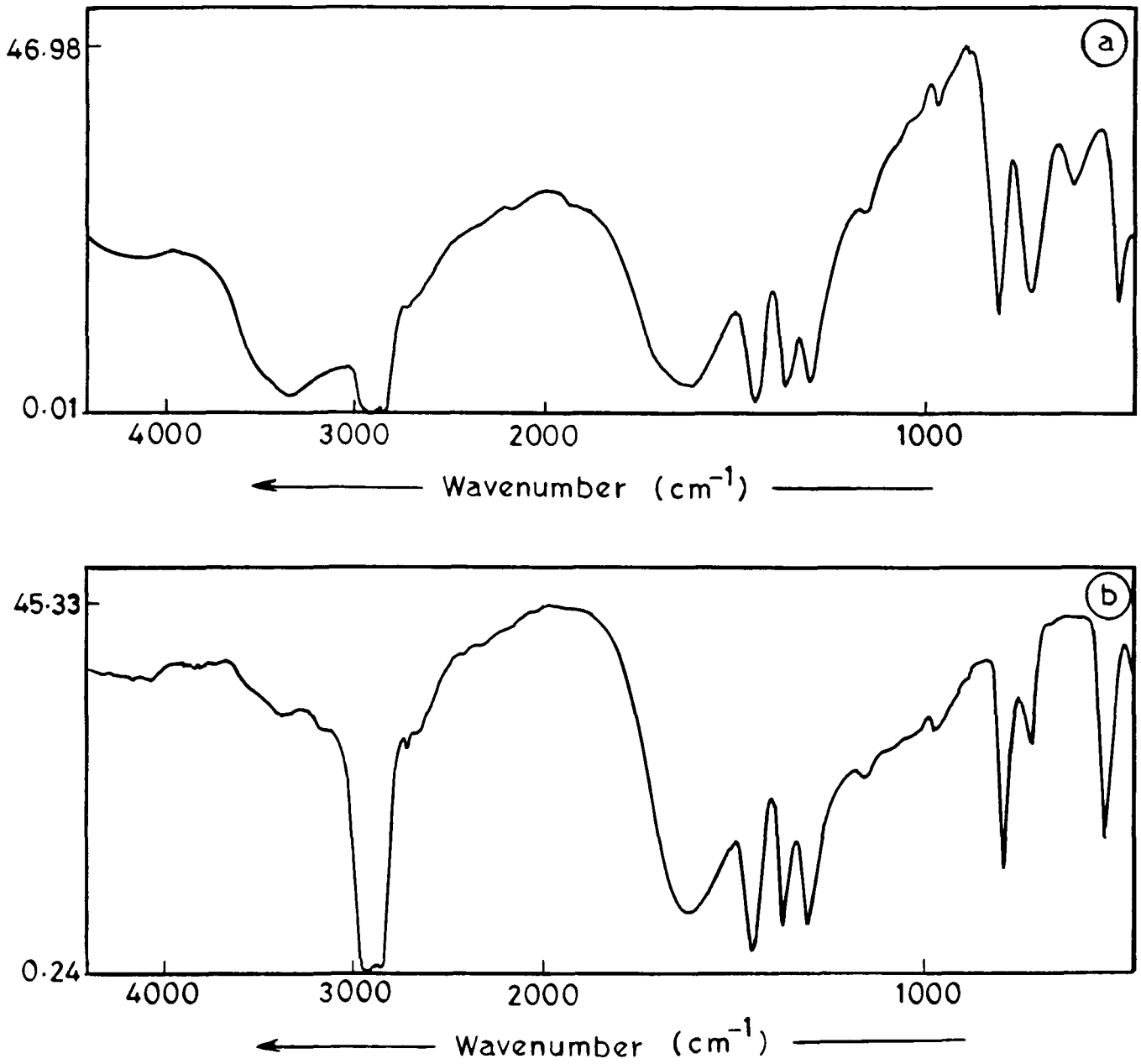

Fig. 1. Infrared spectra of (a) manganese (II) oxalate dihydrate ($MnC_2O_4 \cdot 2H_2O$) and (b) cadmium (II) oxalate monohydrate ($CdC_2O4 \cdot H_2O$).

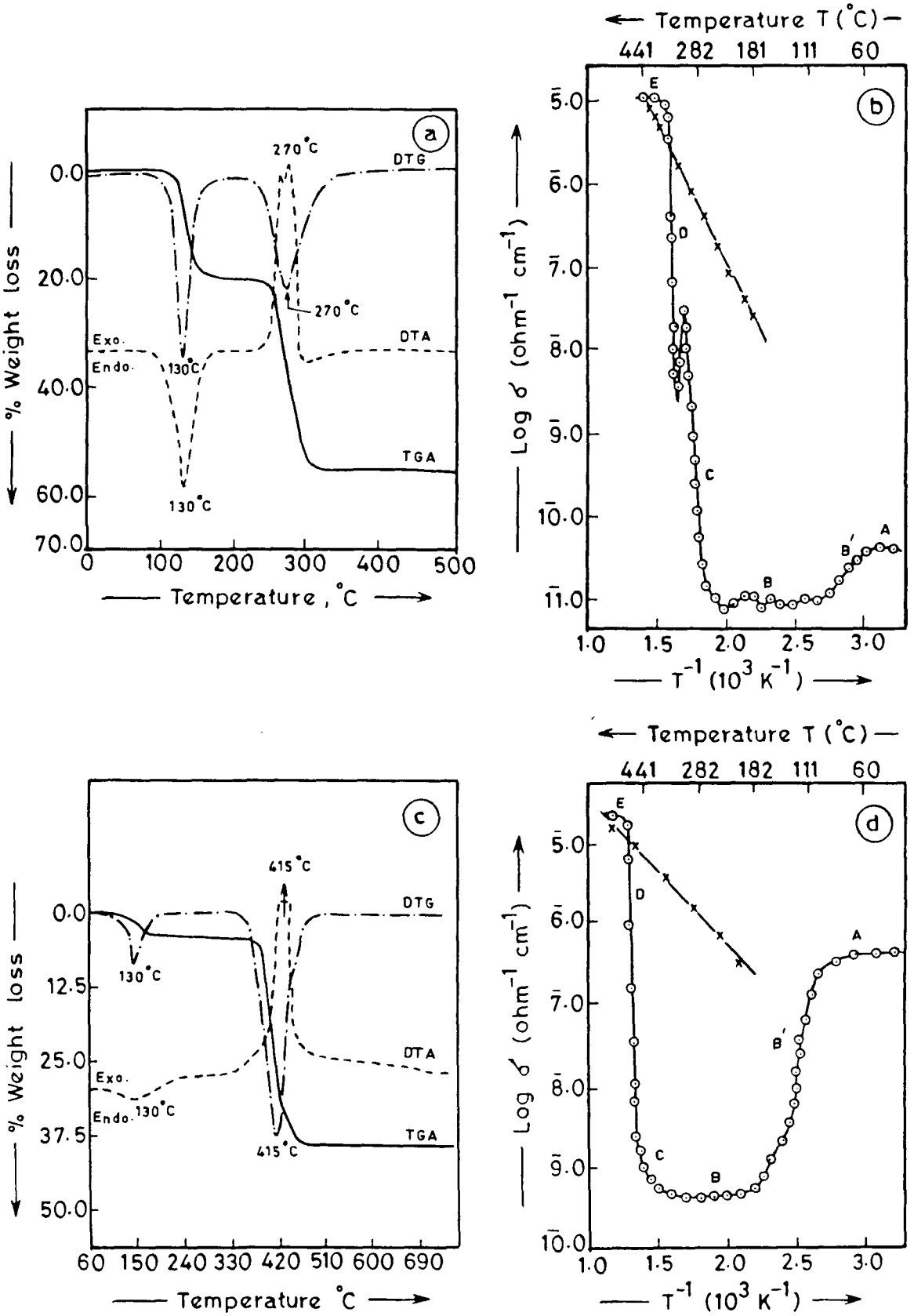

Fig. 2 Thermal decomposition in a static air atmosphere.
(a) TGA, DTG and DTA curves for $MnC_2O_4 \cdot 2H_2O$;
(b) Plot of log σ vs. T^{-1} for $MnC_2O_4 \cdot 2H_2O$:
○, during decomposition; X, cooling cycle;
(c) TGA, DTG and DTA curves for $CdC_2O_4 \cdot H_2O$;
(d) Plot of log σ vs. T^{-1} for $CdC_2O_4 \cdot H_2O$:
○, during decomposition; X, cooling cycle.

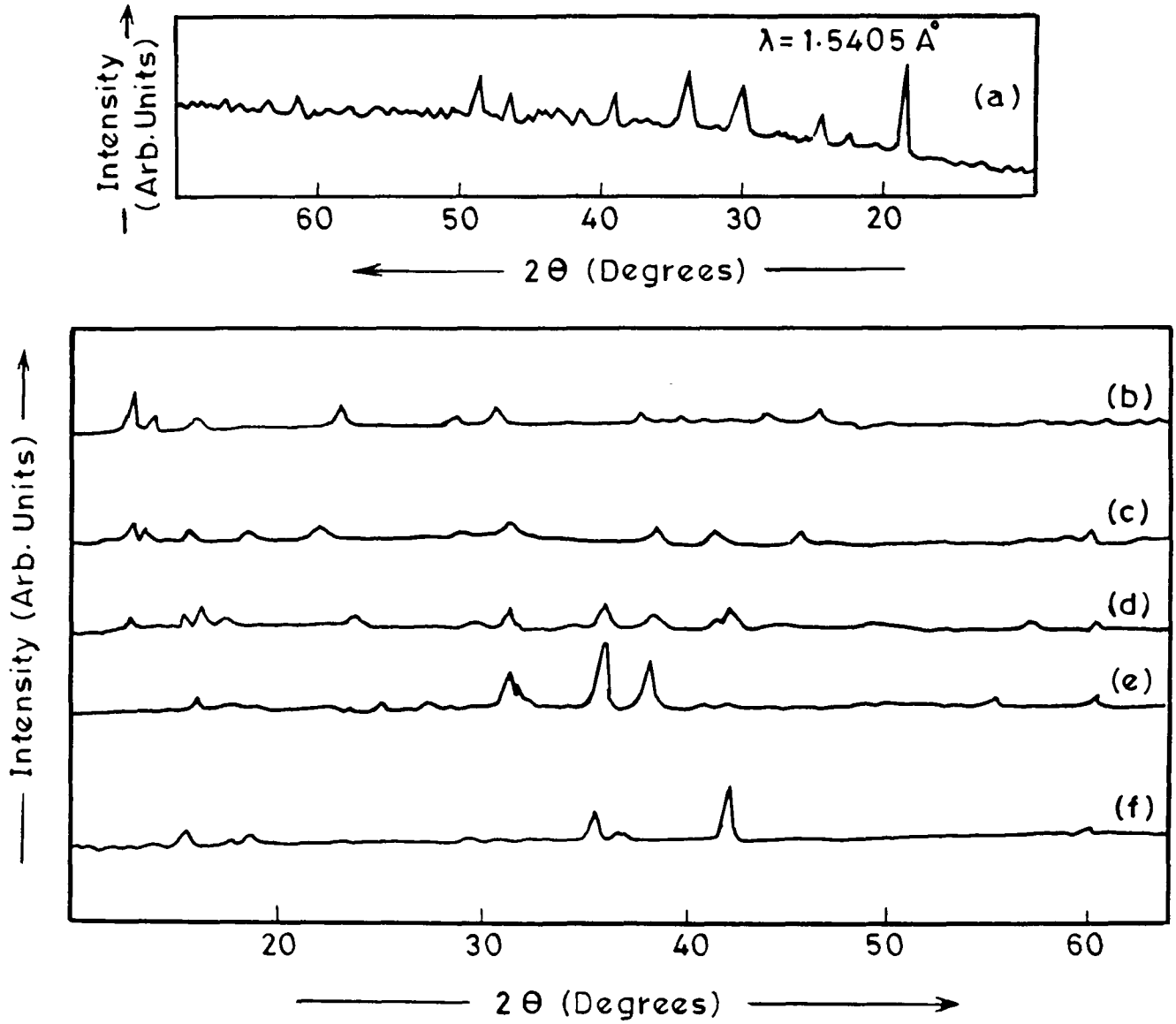

Fig. 3. X-ray diffraction patterns of manganese (II) oxalate dihydrate ($MnC_2O_4 \cdot 2H_2O$) and its decomposed products at various atmospheres. (a) $MnC_2O_4 \cdot 2H_2O$; (b) 225 °C; (c) 290 °C; (d) 340 °C; (e) 360 °C; (f) 450 °C (nitrogen atmosphere).

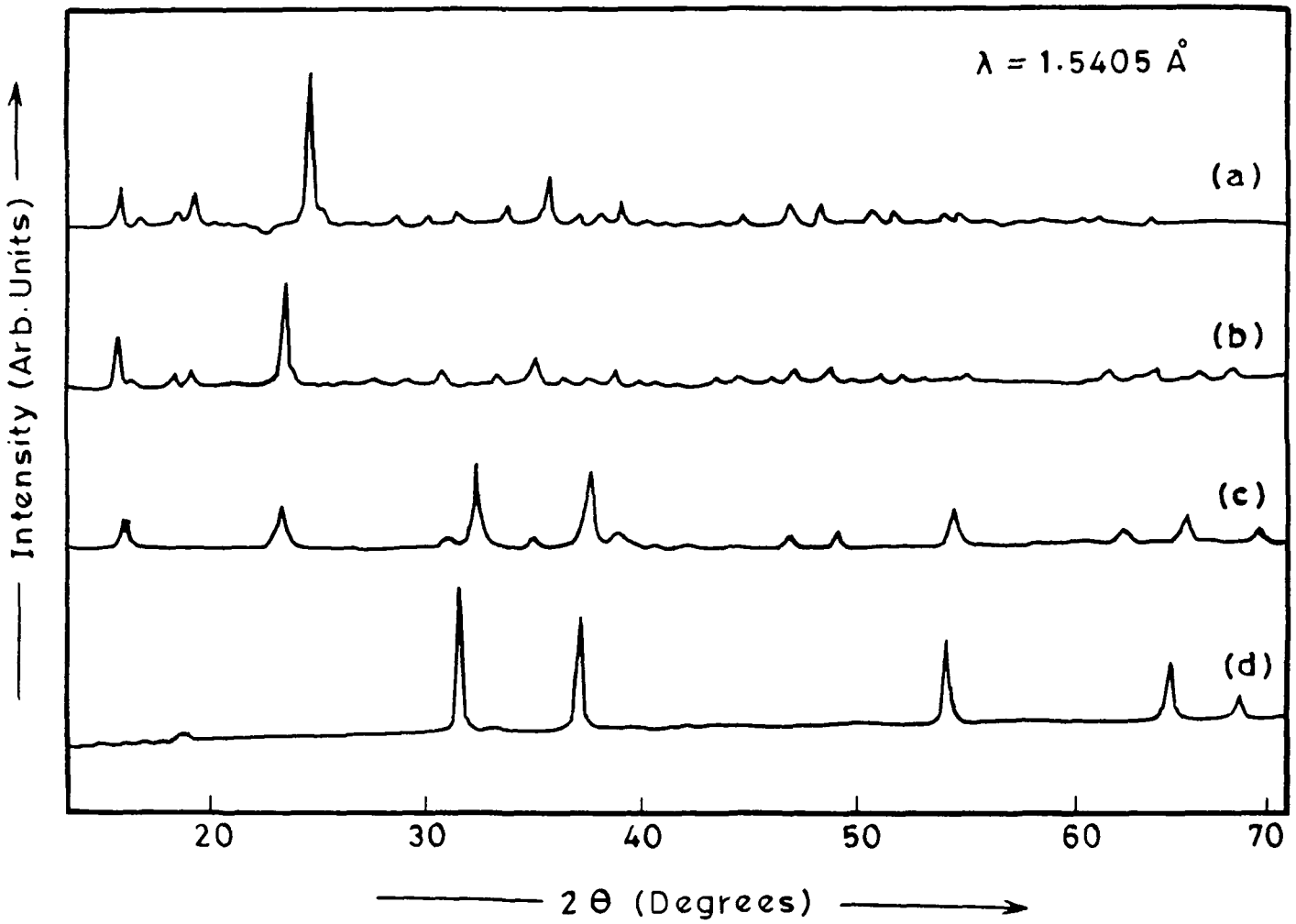

Fig. 4. X-ray diffraction patterns of cadmium (II) oxalate monohydrate ($CdC_2O_4 \cdot H_2O$) and its decomposed products at various temperatures. (a) $CdC_2O_4 \cdot H_2O$; (b) 260 °C; (c) 390 °C; (d) 500 °C (nitrogen atmosphere).

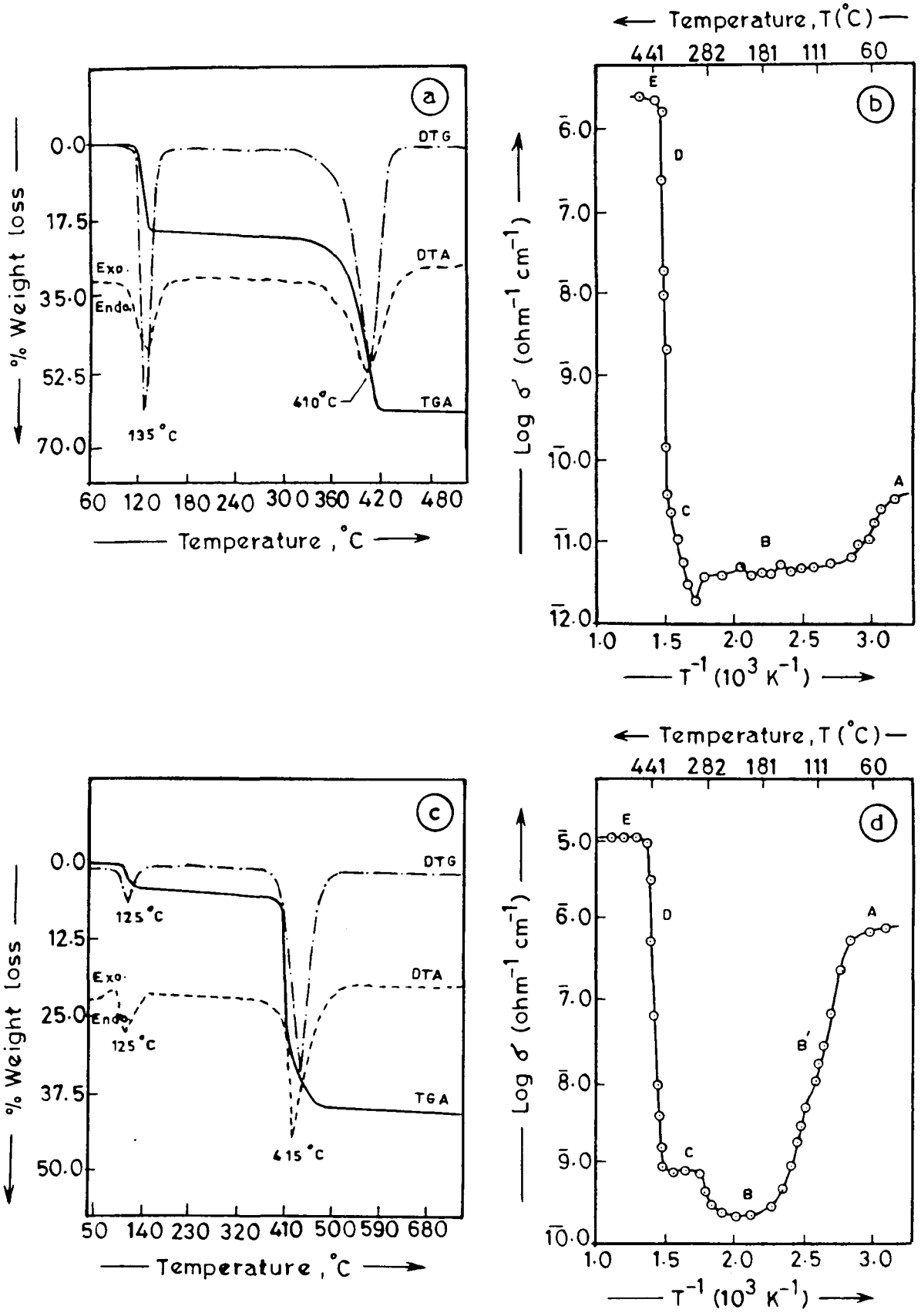

Fig. 5 Thermal decomposition in a dynamic nitrogen atmosphere. (a) TGA, DTG and DTA curves for $MnC_2O_4 \cdot 2H_2O$; (b) Plot of log σ vs. T^{-1} for $MnC_2O_4 \cdot 2H_2O$: o , during decomposition; x , cooling cycle; (c) TGA, DTG DTA curves for $CdC_2O_4 \cdot H_2O$; (d) Plot of log σ vs. T^{-1} for $CdC_2O_4 \cdot H_2O$.

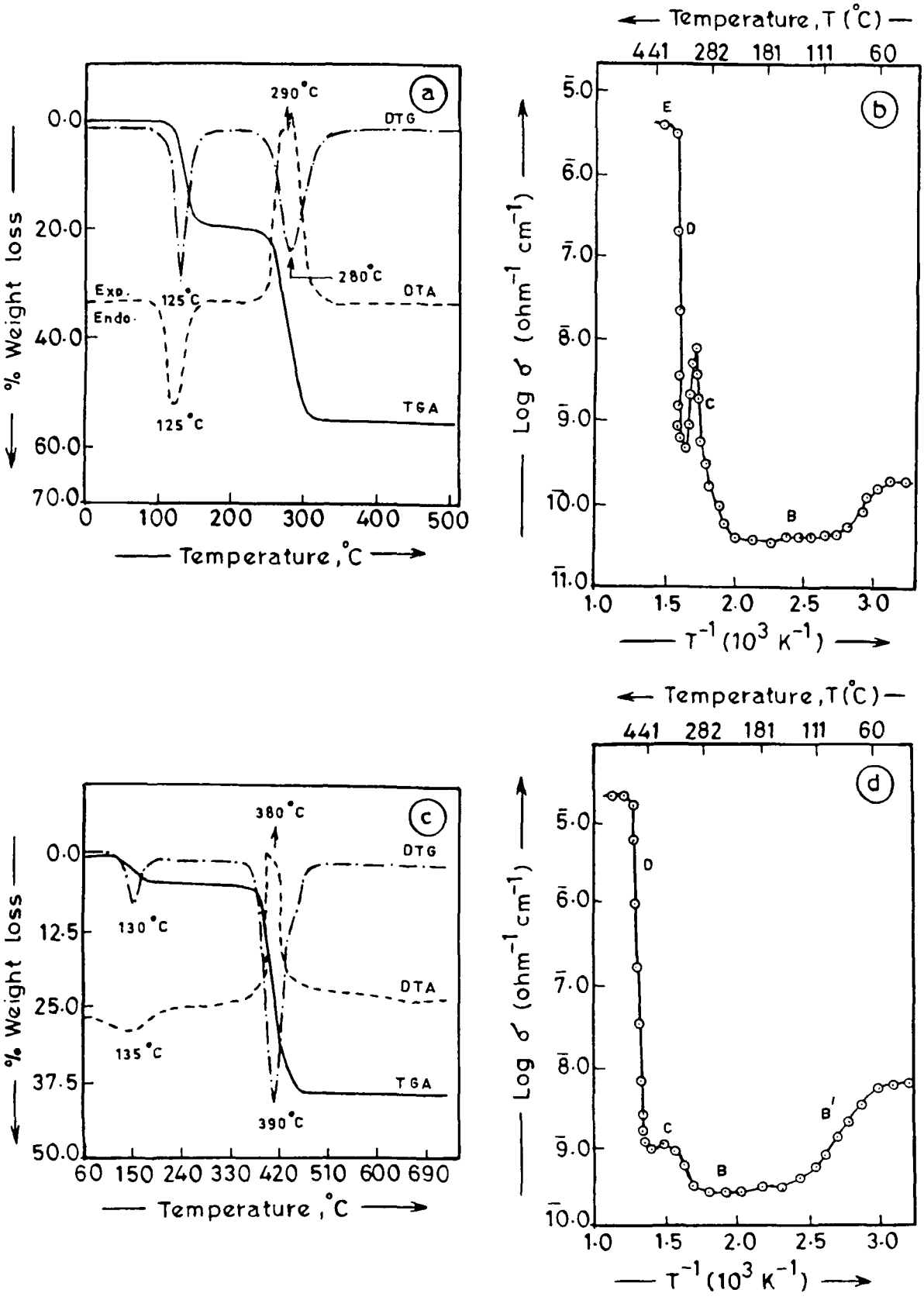

Fig. 6 Thermal decomposition in a dynamic air atmosphere.
(a) TGA, DTG and DTA curves for $MnC_2O_4 \cdot 2H_2O$;
(b) Plot of log σ vs. T^{-1} for $MnC_2O_4 \cdot 2H_2O$;
(c) TGA, DTG and DTA curves for $CdC_2O_4 \cdot H_2O$;
(d) Plot of log σ vs. T^{-1} for $CdC_2O_4 \cdot H_2O$.